Journal of Solid State Chemistry **156,** 267–273 (2001)
doi:10.1006/jssc.2000.8941, available online at http://www.idealibrary.com on IDEAL®

Electronic Structures and Luminescence Properties of $YNbO_4$ and $YNbO_4$:Bi

Seung Kwon Lee,*,†,[1] Hyunju Chang,† Cheong-Hwa Han,‡ Hyun-Jung Kim,†
Ho G. Jang,* and Hee Dong Park†

*Department of Chemistry, Korea University, Seoul, 131-701, Korea; †Advanced Materials Division, Korea Research Institute of Chemical Technology, Taejon, 305-600, Korea; and ‡Department of Chemistry, Halla University, Wonju, 220-712, Korea

Received April 24, 2000; in revised form July 25, 2000; accepted August 17, 2000

The luminescence properties of fergusonite phosphors, $YNbO_4$ and $YNbO_4$:Bi, were investigated with photoluminescence (PL) measurements and first-principles calculations. The various absorption spectra of these phosphors have been interpreted using the calculated partial density of states in the framework of density functional theory. We were able to determine the charge-transfer gap of $YNbO_4$, 4.3 eV, that agrees well with our experimental measurement. From our analysis of PL spectra and calculations, we have investigated the Bi effect in $YNbO_4$:Bi, which shows an excitation peak at a longer wavelength than $YNbO_4$. We have found that the charge transfer from oxygen to bismuth is the main reason for the peak position shift in the excitation spectra. © 2001 Academic Press

Key Words: **$YNbO_4$; density functional theory; blue phosphor; charge transfer.**

INTRODUCTION

Recently, steady improvements have been made in the performance of phosphors specifically for low-voltage applications such as field emission display (FED). Zinc sulfide silver (ZnS:Ag) has been known to be one of the most efficient blue phosphors. However, the sulfide phosphors like ZnS:Ag have disadvantages for FED application due to degradation for low-voltage cathodoluminescence (1). The nonsulfide blue phosphors need to be developed for FED applications. Recently $YNbO_4$:Bi has received attention as a potential blue phosphor for FED (2, 3). $YNbO_4$:Bi showed reasonable cathodoluminescence at low voltage. The host material, $YNbO_4$, itself is a well-known self-activated phosphor showing a broad and strong emission band in the spectral region about 400 nm. Introducing Bi into $YNbO_4$ shifts the emission band to longer wavelength, making $YNbO_4$:Bi a suitable blue phosphor for FED application.

[1]To whom correspondence should be addressed. E-mail: sklee@pado.krict.re.kr. Fax: + 82 42 861 4245.

The luminescent property in $YNbO_4$ is ascribed to the ligand–metal charge-transfer (LMCT) transition of tetrahedral $[NbO_4]^{3-}$ molecular ions (4). Even though $YNbO_4$ itself is a well-known self-activated phosphor, its electronic structure and optical absorption mechanism have not been clearly understood. Therefore, we applied density functional theory (DFT) (5) to analyze the optical absorption characteristics of the host and Bi^{3+} ion as an activator.

In this paper, we present our theoretical calculations on $YNbO_4$ and $YNbO_4$:Bi to interpret their optical absorption. We also discuss the interpretation of their excitation and emission spectra of photoluminescence.

EXPERIMENTAL

$YNbO_4$:Bi phosphors with doping rates between 0.1 and 1.0 wt% have been prepared by the solid-state reaction technique. Y_2O_3 (High Purity Chemical Laboratory Co. Ltd., 99.99%), Nb_2O_5 (High Purity Chemical Laboratory Co. Ltd., 99.99%), and Bi_2O_3 (High Purity Chemical Laboratory Co. Ltd., 99.99%) powders were used as raw materials. The starting materials were weighed out accurately in the required amounts and mixed together using an agate mortar and pestle. During the grinding, a small amount of acetone was added in order to mix the materials homogeneously. The samples were fired in Al_2O_3 crucibles at 1250–1400°C for 2–24 hours in air. In the present investigation, we have used the samples of undoped $YNbO_4$ and 0.2 wt% Bi^{3+}-doped $YNbO_4$.

Optical measurements were performed using a Perkin Elmer LS 50 luminescence spectrometer at room temperature. The samples were excited with 227 or 310 nm radiation and the emission wavelength was scanned from 300 to 625 nm at a scanning rate of 100 nm/min.

Samples were checked by X-ray powder diffraction (XRD, Rigaku DMAX-33 X-ray diffractometer) and found to be of a single phase.

0022-4596/01 $35.00

COMPUTATIONAL DETAILS

The cluster method within the framework of density functional theory (DFT) is utilized in the present studies on the electronic structure of the host materials and the effect of an activator. This cluster method has been known to be useful for investigating the local properties of impurities and defects in the solid state (6). A cluster can be considered as a group of atoms, which are chosen in such a manner that one can describe adequately the local environment of the atoms of concern. With a large number of point charges, one can simulate the effect of the rest of bulk material on this cluster. We have carried out the cluster calculations for $YNbO_4$ and the $YNbO_4$:Bi. Each cluster includes a central ion of interest and its nearest neighbors. The space is partitioned into a cluster region (region I) and an environmental region (region II). Inside region I, Kohn–Sham equations are solved numerically. In region II, Madelung potential is approximately taken into account with point charge distribution. As shown in Fig. 1, the Nb-centered 35-atom cluster was embedded in a 304-point charge environment to represent the $YNbO_4$ crystal (7). The structure of $YNbO_4$ was taken from Ref. (8). All the atoms within a radius of 4 Å around the Nb^{5+} ion were included in the cluster. A Bi-centered 33-atom cluster (Bi substituting Y) was taken for $YNbO_4$:Bi. Single-point DFT calculations were carried out as implemented in the $DMol^3$ program package (9) from Molecular Simulation Inc. We have taken a nonlocal density approximation, the so-called generalized gradient approximation (GGA) functional suggested by Perdew and Wang (10). As the basis sets, we have used double numerical basis functions with polarization functions (DNP) for all the calculations (11). The relativistic effective core potential (ECP) approximation was used for the core electrons of Y, Nb, and Bi. All cluster and periodic calculations were carried out in the spin-restricted model.

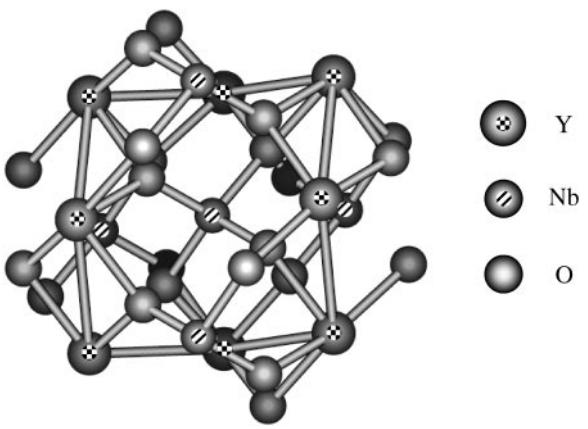

FIG. 1. Structure of the 35-atom Nb-centered cluster in $YNbO_4$.

RESULTS AND DISCUSSION

There is a wealth of optical data for $YNbO_4$ and $YNbO_4$:Bi phosphors. We review some of the experimental results relevant to our analyses of the electronic structure of these phosphors. We also interpret our new experimental data. The band gaps of $YNbO_4$ and $YNbO_4$:Bi were determined by Grisafe and Fritsch (4) to be 4.3 and 3.6 eV from diffuse reflectance spectra, respectively. Similar results were obtained by Blasse and Bril (12) and Harrison and Blasse (13).

$YNbO_4$ has the fergusonite structure and $[NbO_4]^{3-}$ groups have distorted tetrahedral coordination (8). If we assume these groups to be undistorted tetrahedra, the external configuration of $[NbO_4]^{3-}$ in the ground state is $(1a_1)^2(1t_2)^6(1e)^4(2t_2)^6(1t_1)^6$, and the sequence of the excited orbitals is $2e < 3t_2 < 4t_2 < 2a_1$ (14). Here the filled orbitals are concentrated on the oxygen ions and the empty ones on the niobium ions, so that the lowest optical transitions can be considered as $2p$(O)–$4d$(Nb) charge-transfer transitions, $t_1 \rightarrow 2e$. Thus, the excited state consists of an increased electron density in the vicinity of the metal ion, along the tetrahedral bonds. The ground state t_1^6 is a state of symmetry $^1A_1$, and the excited state $t_1^5e^1$ produces the following states, $^3T_2$, $^3T_1$, $^1T_1$, and $^1T_2$. The actual site symmetry of niobate tetrahedra in fergusonite is C_2. The $^3T_1$ level is split into one A and two B levels because of lowering of the crystal field symmetry from T_d and including the spin–orbit interaction. The order of these levels is $^1T_2 > {}^1T_1 > {}^3T_2 \geq {}^3T_1$. Electronic levels and their assignments are given schematically in Fig. 2 for the $[NbO_4]^{3-}$ molecular ion, assuming a tetrahedral environment.

Only the transition $^1A_1 \rightarrow {}^1T_2$ is allowed as an electric–dipole transition. In addition to the electric–dipole transition, $^1T_1$–$^1A_1$, $^3T_1$–$^1A_1$, and $^3T_2$–$^1A_1$ also have a certain nonvanishing transition probability. The singlet–triplet transition can acquire intensity from the allowed transition by spin-orbit coupling. The $^3T_1$–$^1A_1$, and $^3T_2$–$^1A_1$ transitions will have the higher transition probability for the stronger spin–orbit coupling interaction. The $^1T_1$–$^1A_1$ transition will become more intense for the larger deviation from a cubic symmetry. In view of this point, we can assign the first strong absorption band in order of increasing energy to $^1A_1 \rightarrow {}^3T_1$, $^3T_2$, $^1T_1$ transitions and the second one to the $^1A_1 \rightarrow {}^1T_2$ transition in the excitation spectra of $YNbO_4$, as shown in Fig. 3a.

In Fig. 3, curves a and b show the different absorption edges for $YNbO_4$ and $YNbO_4$:Bi, which are assigned to 280 nm (4.4 eV) and 330 nm (3.8 eV), respectively. Comparing the excitation spectra of $YNbO_4$ and $YNbO_4$:Bi, the band shape and peaking position are well matched in the region from 200 nm to 280 nm. But $YNbO_4$:Bi has a new peak around 310 nm. Obviously this is a Bi effect that influences the optical properties of the niobate group. The

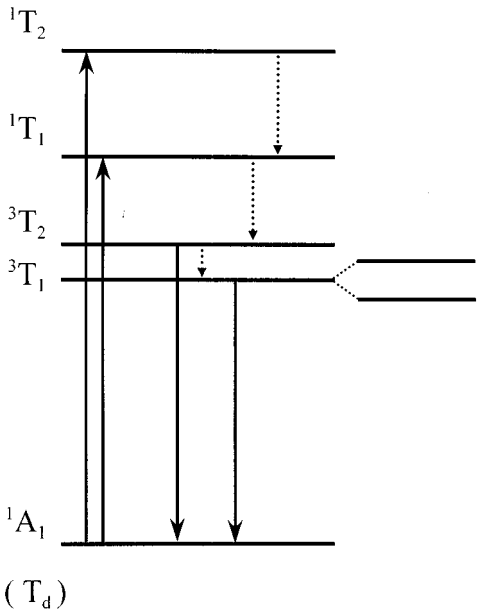

FIG. 2. Four-level energy diagram for absorption and luminescence processes of the $[NbO_4]^{3-}$ molecular ion in the tetraheral structure.

Bi^{3+} ions in $YNbO_4$ have two possible optical transitions. First, Bi^{3+} ion can directly absorb the incident electromagnetic radiation. The ground state of a free ion of Bi^{3+} is the $^1S_0$ state with a $6s^2$ configuration. The excited levels can be $^3P_0$, $^3P_1$, $^3P_2$, and $^1P_1$ states (in sequence of increasing energy) with a $6s6p$ configuration. The transitions from $^1S_0$ to $^3P_0$ and $^3P_2$ are completely spin forbidden, if no other configurations are taken into account. The two levels, $^3P_1$ and $^1P_1$, are mixed by spin–orbit coupling. Therefore, only the transitions $^1S_0 \rightarrow {}^3P_1$ and $^1S_0 \rightarrow {}^1P_1$ are expected to have a reasonable absorption intensity. Second, the charge-transfer transition from the O^{2-} ion to the empty $6p$ level of the Bi^{3+} ion is possible. Generally the former is known to occur easily in many cases. However, we suggest that charge transfer is dominant in $YNbO_4$:Bi on the basis of the following reasons.

Materials such as $YNbO_4$ are the phosphors with 100% center concentration (15); thus, all niobate groups may be considered as fluorescent centers. If the Bi^{3+} ions are internally excited, the $YNbO_4$:Bi has stronger excitation intensity than $YNbO_4$, because internal transitions of the Bi^{3+} ions are in addition to the charge-transfer transition of the niobate groups. But we found that the integration areas of the excitation spectra were approximately the same for both $YNbO_4$ and $YNbO_4$:Bi phosphors. This implies that the emissions from $YNbO_4$ and $YNbO_4$:Bi are approximately the same, considering that the quantum efficiencies of $YNbO_4$ and $YNbO_4$:Bi are $\sim$45% (16) and $\sim$40% (17), respectively.

The emission spectra of $YNbO_4$ and $YNbO_4$:Bi are shown in Fig. 4. Under 227 nm excitation, the excitation energy is larger than the charge-transfer gap energy of $YNbO_4$; thus, emissions from both $YNbO_4$ and $YNbO_4$:Bi are possible. The emission band of $YNbO_4$:Bi has a maximum at 420 nm, while that of $YNbO_4$ has a maximum at 400 nm. However, under 310 nm excitation, which is slightly larger than the transition energy of Bi^{3+}, only the emission spectrum of the $YNbO_4$:Bi shows a broad band with a maximum at 447 nm (curve b″ in Fig. 4). This difference in the emission spectra can be ascribed to the Bi effect. Therefore, curve b′ of $YNbO_4$:Bi in Fig. 4 can be split into two emission peaks. We have done Gaussian fitting on curve b′, which is well separated into two peaks at 406 and 448 nm as shown in Fig. 5. These two peaks, (1) and (2) in Fig. 5, agree well

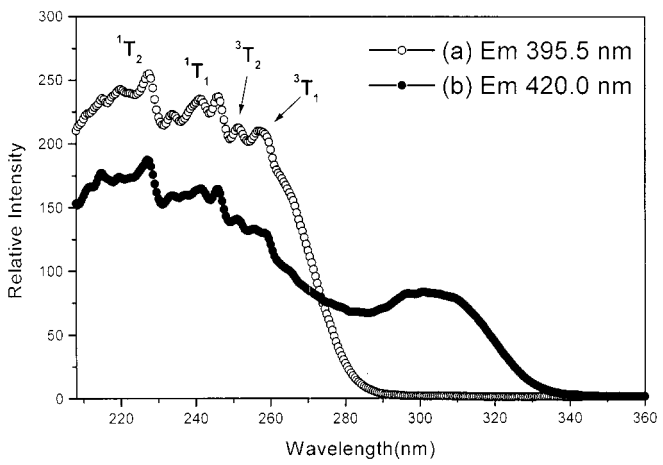

FIG. 3. Relative excitation spectra of $YNbO_4$ (curve a) emission ($\lambda = 395.5$ nm) and $YNbO_4$:Bi (0.2 wt% Bi^{3+} doped) (curve b) emission ($\lambda = 420$ nm).

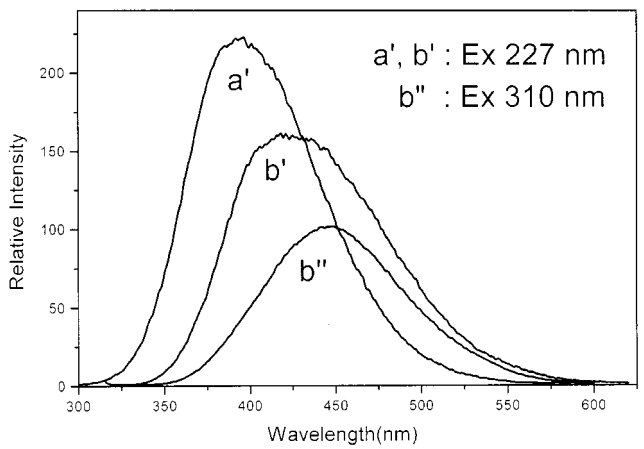

FIG. 4. Spectral–energy distribution of the emission at room temperature: (a′) $YNbO_4$ under 227 nm excitation, (b′) $YNbO_4$:Bi (0.2 wt% Bi^{3+} doped) under 227 nm excitation, and (b″) $YNbO_4$:Bi (0.2 wt% Bi^{3+} doped) under 310 nm excitation.

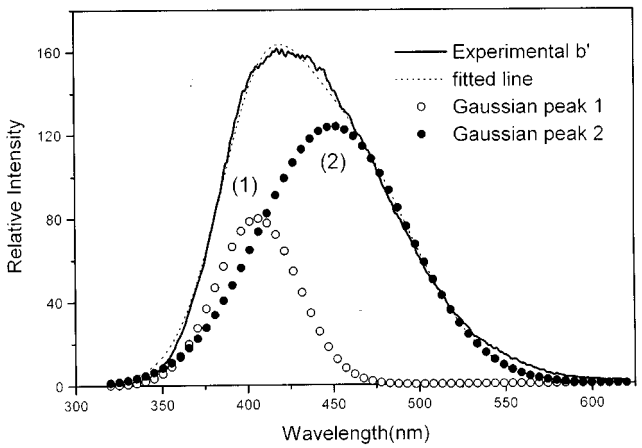

FIG. 5. Fitted emission spectra of $YNbO_4$:Bi (0.2 wt% Bi^{3+} doped) under 227 nm excitation (curve b′ in Fig. 4).

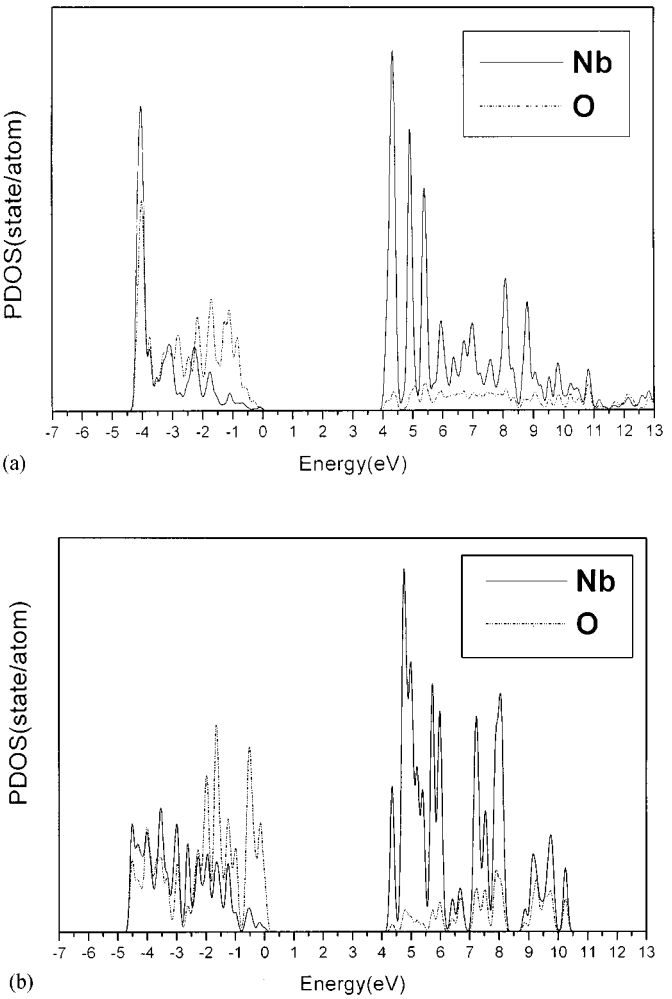

FIG. 6. (a) Partial density of states (PDOS) of $YNbO_4$ from the Nb-centered cluster. (b) Partial density of states (PDOS) of $YNbO_4$ from periodic calculation.

with the host peak (curve a′) and the Bi peak (curve b″) in Fig. 4, respectively. The areas of the two peaks are integrated; the Bi part is 80%, whereas the host part is 20%. It implies that the emission in $YNbO_4$:Bi (curve b′ in Fig. 4) dominantly consists of the emission from Bi.

For the host material $YNbO_4$, the calculated partial densities of states (PDOS) of the central Nb and the nearest neighboring O are shown in Fig. 6a. The PDOS is broadened by a Gaussian function with a width of 0.1 eV. Even though the curves of Fig. 6 do not correspond directly to the spectra, the difference between the peaks of these PDOS plots is related to the absorption spectra. The charge-transfer gap between Nb and O is clearly shown in Fig. 6a. The valence band (VB) consists of mainly the O 2*p* orbital and the conduction band (CB) of the Nb 4*d* orbital. The band gap is estimated as 4.3 eV, which agrees well with our experimental result (4.4 eV) and others (4.3 eV) (4, 12, 13). The PDOS of Y is away from the region we are interested in; thus, we do not give any attention to them in the present report. We have also performed a periodic calculation on $YNbO_4$, which contains 24 atoms in the conventional unit cell, in order to verify the reliability of our cluster model. As shown in Fig. 6b, periodic model and cluster model calculations give roughly similar results. It implies that our cluster method can give reliable results in a bulk system like a periodic method can do, then we can safely apply the cluster method for a defect system like $YNbO_4$:Bi, avoiding computationally expensive periodic calculations.

A similar cluster method was applied to $YNbO_4$:Bi to investigate the effect of introducing Bi at the Y site. When Bi^{3+} replaces Y^{3+}, lattice distortion around Bi is expected since the ionic radius of Bi^{3+} is larger than that of Y^{3+}. Therefore, we have carried out geometry optimization of $YNbO_4$:Bi. We took a supercell of 48 atoms, twice the conventional unit cell, in which one Y atom is replaced with Bi; thus, the supercell is large enough that the impurity–impurity interaction is minimized. We then optimized the geometry of the supercell using the FastStructure program (18). Optimization was terminated when residual forces were less than 0.0001 a.u., the displacement change was less than 0.0003 a.u., and the energy change was less than 10^{-6} a.u. Geometry optimization data are summarized in Tables 1 and 2.

The Y site, before the Bi ion is substituted, has 12 cations within 4 Å: upper cations, Y[9, 10], Nb[5, 6]; middle cations, Nb[1, 2, 3, 4]; and lower cations, Y[11, 12] and Nb[7, 8] (see Fig. 7). Upper and lower cations locate at nearly equivalent distances. However, the plane, containing four niobiums (middle cations), lies slightly beneath the Y center. So when Bi^{3+} substitutes for Y^{3+}, the Bi site is expanded toward lower cations. The distances of Bi–O[17, 18, 19, 20] increase, whereas those of Bi–O

TABLE 1
Geometry Optimization Results: Selected Bond Distance (Index number in Fig. 7)

Distance (Å)	Before optimiation, R_b	After optimizations, R_a	Deviation, $\Delta R = R_a - R_b$
Bi–Nb(1)	3.828	3.857	0.029
Bi–Nb(2)	3.538	3.577	0.039
Bi–Nb(3)	3.828	3.875	0.047
Bi–Nb(4)	3.538	3.577	0.039
Bi–Nb(5)	3.877	3.611	− 0.266
Bi–Nb(6)	3.877	3.667	− 0.210
Bi–Nb(7)	3.701	3.962	0.261
Bi–Nb(8)	3.701	4.018	0.317
Bi–Y(9)	3.804	3.554	− 0.250
Bi–Y(10)	3.804	3.668	− 0.136
Bi–Y(11)	3.768	4.043	0.275
Bi–Y(12)	3.768	4.122	0.354
Bi–O(13)	2.340	2.223	− 0.117
Bi–O(14)	2.397	2.240	− 0.157
Bi–O(15)	2.397	2.240	− 0.157
Bi–O(16)	2.340	2.338	− 0.002
Bi–O(17)	2.401	2.675	0.274
Bi–O(18)	2.313	2.731	0.418
Bi–O(19)	2.401	3.055	0.654
Bi–O(20)	2.313	2.731	0.418

[13, 14, 15, 16] decrease. Two angles of O[14]–Bi–O[20] and O[15]–Bi–O[18] are getting close to 180°. In consideration of the angles, the orbital overlap between Bi and O[14, 15, 18, 20] may increase. The distances of Bi–O [18, 20] are longer than those of Bi–O[14, 15] and the distance of Bi–O[13] is the shortest. Therefore, the charge transfer between Bi and O[13, 14, 15, 16] may occur more easily than that between Bi and the other oxygen in view of distances and angles.

TABLE 2
Geometry Optimization Results: Selected Angle of Oxygen–Metal (Bismuth)–Oxygen (Index Numbers in Fig. 7)

Radiant	Before optimization, A_b	After optimization, A_a	Deviation $\Delta A = A_a - A_b$
O(13)-Bi–O(15)	72.5	85.9	13.4
O(13)–Bi–O(16)	133.7	142.8	9.1
O(13)–Bi–O(19)	156.5	144.2	− 12.3
O(13)–Bi–O(20)	107.3	107.1	− 0.2
O(14)–Bi–O(15)	82.6	87.6	5.0
O(14)–Bi–O(16)	72.5	79.6	7.1
O(14)–Bi–O(19)	120.6	122.1	1.5
O(14)–Bi–O(20)	156.9	175.0	18.1
O(15)–Bi–O(17)	120.6	127.4	6.8
O(15)–Bi–O(18)	156.9	175.0	18.1
O(16)–Bi–O(17)	156.5	150.8	− 5.7
O(16)–Bi–O(18)	107.3	111.9	4.6

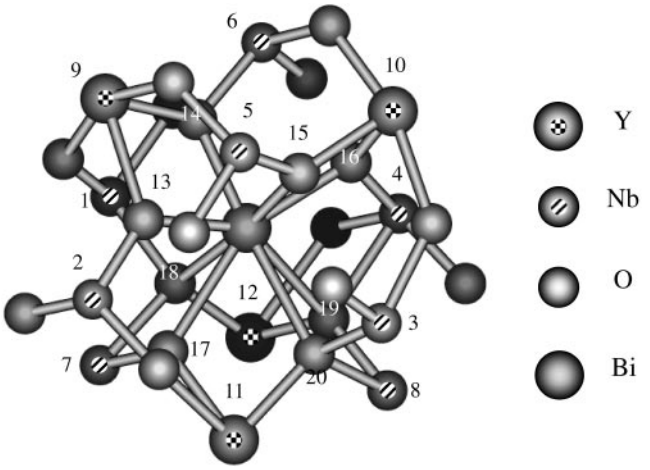

FIG. 7. Structure of the 33-atom Bi-centered cluster in $YNbO_4$:Bi when Bi substitutes Y. The index numbers in the atoms correspond to the index numbers in Tables 1 and 2.

For $YNbO_4$:Bi, we started the cluster calculations with DMol[3] from the above optimized geometry. A Bi-centered 33-atom cluster, as shown in Fig. 7, was embedded in 241 point charges. When we treat Bi as a point defect, the local geometry around Bi is distorted from the crystal structure of $YNbO_4$. Therefore, the atomic positions of the point charge environment are fixed to be the same as those in $YNbO_4$, whereas the atomic positions of the Bi-centered cluster are taken from the optimized geometry.

The calculated PDOS of the central Bi and the nearest neighboring O are shown in Fig. 8 with the PDOS of Nb, which is calculated from the Nb-centered cluster. The $2p(O^{2-})$ valence band levels lie slightly above the $6s(Bi^{3+})$

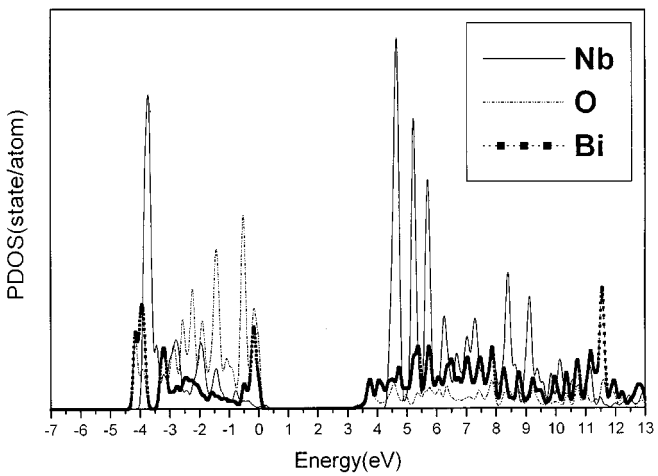

FIG. 8. Partial density of states (PDOS) of $YNbO_4$:Bi from the Bi-centered cluster.

levels in the valence band. The charge density distribution of the highest occupied molecular orbital (HOMO) in Fig. 9 also shows that the $2p(O^{2-})$ density is higher than that of the $6s(Bi^{3+})$. In the conduction band, the PDOS of $6p(Bi^{3+})$ is located at a lower energy than the PDOS of $4d(Nb^{5+})$ by about 0.8 eV. It causes the energy gap in $YNbO_4$:Bi to decrease: i.e., adding Bi^{3+} ions to $YNbO_4$ makes the emission peak move toward longer wavelength (19).

Since $2p(O^{2-})$ and $6s(Bi^{3+})$ levels are overlapped in the valence band, the absorption mechanism of $YNbO_4$:Bi can involve both [Bi–O] and [Nb–O] charge-transfer transitions. The electrons of O can transfer not only to Nb but also to Bi in $YNbO_4$:Bi. This is in agreement with that the transition probability of [Nb–O] group charge transfer is decreased when the compound is doped with Bi^{3+}, which was discussed earlier with the integration areas of the excitation spectra. One-dimensional scheme is illustrated in Fig. 10.

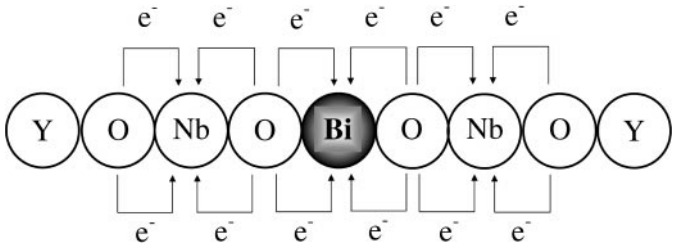

FIG. 10. One-dimensional charge-transfer transition scheme when Bi substitutes in the Y site.

SUMMARY

We have analyzed the excitation and emission spectra of $YNbO_4$ and $YNbO_4$:Bi phosphors. As we controlled the excitation energies, we were able to separate the host part and the bismuth part in the emission spectra. We have found that the emission from the host was reduced when Bi was doped. This strongly suggests that the electrons of oxygen can transfer not only to Nb but also to Bi in $YNbO_4$:Bi.

We have performed first-principles calculations within the density functional formalism in order to analyze the electronic structure of $YNbO_4$ and $YNbO_4$:Bi. From the calculated partial density of states (PDOS), we can determine the charge-transfer gap of $YNbO_4$ between O 2*p* and Nb 4*d*, which agrees well with the experiment. We have calculated the doping effect of Bi activator in $YNbO_4$:Bi. The calculated PDOS of Bi shows that the Bi 6*p* lies below the Nb 4*d* energy levels, then it reduces the band gap and makes the peak shift to longer wavelength in the excitation spectra of $YNbO_4$:Bi. Though the valence band of $YNbO_4$:Bi consists of mainly O 2*p* and Bi 6*s*, the HOMO has more O 2*p* character than Bi 6*s* character. It indicates that the charge transfer from O 2*p* to Bi 6*p* can occur easily in $YNbO_4$:Bi. We have also investigated structural relaxation around Bi in the $YNbO_4$ lattice using a geometry optimization method, and found some changes in the distances between Bi and O. This structural relaxation seems to enhance the charge transfer between Bi and O. From the analysis of PL excitation spectra and theoretical calculations, we can conclude that the charge transfer between O 2*p* and Bi 6*p* is dominant in $YNbO_4$:Bi. This charge transfer causes the peak shift to the longer wavelength to emission spectra; thus, $YNbO_4$:Bi can be a candidate for blue phosphor of FED application.

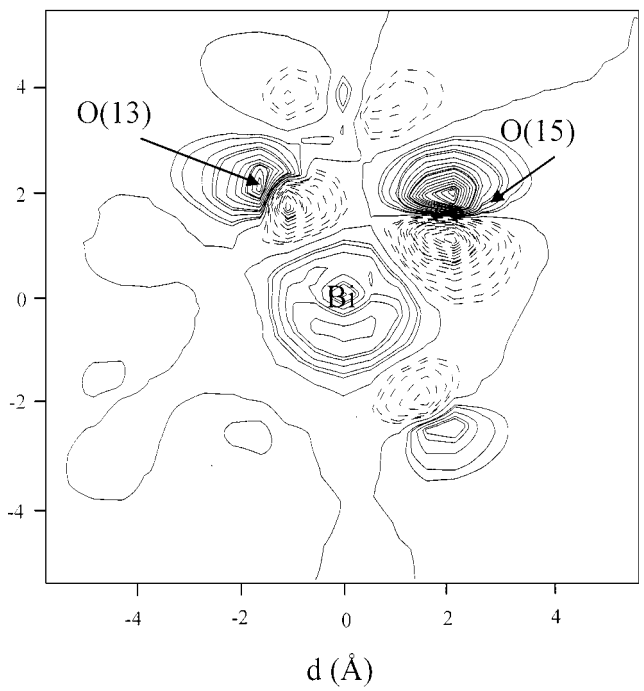

FIG. 9. Charge density distribution of HOMO in the Bi-centered cluster of $YNbO_4$:Bi.

ACKNOWLEDGMENT

This work was supported financially by the Ministry of Science and Technology in Korea.

REFERENCE

1. S. Itoh, T. Kimizuka, and T. Tonegawa, *J. Electrochem. Soc.* **136**(6), 1819 (1989).
2. A. Vecht, D. Charlesworth, and D. W. Smith, *SID. 97 DIGEST*. 588 (1997).
3. X. Jing, C. Gibbons, D. Nicholas, J. Silver, A. Vecht, and Ch. S. Frampton, *J. Mater. Chem.* **9,** 2913 (1999).
4. D. A. Grisafe and C. W. Fritsch, *J. Solid State Chem.* **17,** 313 (1976).
5. W. Kohn and L. J. Sham, *Phys. Rev. A* **140,** 1133 (1965).

6. D. E. Ellis and J. Guo, "Density Functional Theory of Molecules, Clusters and Solids," pp. 263–309. Kluwer Academic, Dordrecht, 1995.
7. The number of cluster atoms was taken after checking the convergence of local properties (Mulliken charges, band gap, and PDOS) of the central Nb and the nearest O's (or the central Bi and the nearest O's), as increasing the size of the cluster. The point charge distribution has been also determined in the same manner.
8. H. Weitzel and H. Schröcke, *Z. Kristallogr.* (in German), **152,** 69 (1980).
9. DMol^3, User's Reference, Molecular Simulation Inc., San Diego, 1998.
10. J. P. Perdew and Y. Wang, *Phys. Rev. B* **45,** 13244 (1992).
11. P. Hébant and G. S. Picard, *J. Mol. Struct.* (*Theochem*) **358,** 39 (1995).
12. G. Blasse and A. Bril, *J. Chem. Phys.* **48,** 217 (1968).
13. D. E. Harrison and G. Blasse, *J. Electrochem. Soc.* **110,** 23 (1963).
14. A. S. Marfunin, "Physics of Minerals and Inorganic Materials (An Introduction)," p. 119. Springer-Verlag, Berlin, 1979.
15. G. Blasse, *Philips Res. Rep.* **23,** 344 (1968).
16 G. Blasse, *J. Electrochem. Soc.* **115**(10), 1067 (1968).
17. G. Blasse and A. Bril, *J. Chem. Phys.* **48**(1), 217 (1968).
18. J. Harris, R. O. Jones, and J. E. Müller, *J. Chem. Phys.* **75,** 3904 (1981).
19. C. H. Han, H. J. Kim, and H. D. Park, *J. Kor. Ceram. Soc.* (in Korean) **36,** 319 (1999).